Diffuse scattering from liquid solutions with white-beam undulator radiation for photoexcitation studies†

Anton Plech,[a]* Rudolf Randler,[a] Armin Geis[b] and Michael Wulff[a]

[a]European Synchrotron Radiation Facility, BP 220, 38043 Grenoble, France, and [b]Laboratoire de Spectrométrie Physique, Université Joseph-Fourier Grenoble I, CNRS (UMR 5588), BP 87, F-38402 St Martin d'Hères, France. E-mail: plech@esrf.fr

Scattering from molecules in solution is a natural way to study fast reactions in solution with X-ray probes. With the availability of reliable femtosecond laser systems and pulsed synchrotron sources with high brilliance, it has become possible to study picosecond time-resolved photoexcitation in condensed matter. Owing to the low scattering cross section and the high background from the non-excited solvent, high flux and long exposure times are required to obtain information about isolated molecules in the conventional monochromatic scattering scheme. It is proposed that the full spectrum of a single-line undulator be used to obtain the diffuse scattering distribution. The bandwidth of 2–5% of the first harmonic, which is easily achievable in current insertion devices, is sufficient to allow the derivation of molecular form factors even in diluted systems. The relaxed bandwidth augments the usable flux drastically.

Keywords: diffuse scattering; liquid solutions; undulator radiation.

1. Introduction

Studies of chemical reactions or dynamic phenomena in condensed matter have benefited tremendously from ultrafast pump-and-probe techniques. The rapid development of short-pulse laser systems allowed the excitation of a photosensitive system with intense laser pulses as short as tens to hundreds of femtoseconds. The transient change of the states can be probed by a second pulse that is delayed with respect to the excitation pulse by a chosen time interval. One can derive structural information from the absorption spectrum when the electronic states of the reactants are well known.

A more direct way of extracting structural information from the system is by using hard X-rays as probe radiation. This can, for example, be realized by femtosecond (laser-driven) X-ray plasma sources. At present, these still suffer from low flux and brilliance. For the case of reactions of molecules in liquid solutions, which is a very relevant area in femtochemistry, we will demonstrate that a considerably high flux is needed to discern the photo-signal from the solvent background.

On the other hand, third-generation synchrotrons can naturally provide pulsed radiation at a much higher flux and brilliance level than table-top systems. A time resolution in the picosecond range can thereby be achieved. Experimental set-ups have been realized, for example, at the Advanced Photon Source, the Advanced Light Source and the European Synchrotron Radiation Facility (ESRF). At the beamline ID09B at ESRF, an instrument has been built to photoexcite samples from an intense femtosecond laser source and probe the structure with synchronized X-ray pulses at a chosen time delay.

Some experiments have already proven that structural studies on small dissolved molecules are feasible (Neutze *et al.*, 2001; Geis *et al.*, 2001). Still, the subtle changes in scattering require long exposure times as the monochromatic X-ray flux still limits the signal-to-noise ratio. We propose a scheme to relax the bandwidth used for diffuse wide-angle scattering by using the natural line width of a single-line undulator, which in turn boosts the usable flux by more than two orders of magnitude.

Table 1
Characteristics of the femtosecond laser system.

Fundamental wavelength	800 nm	3×10^{15} photons/pulse
Frequency doubling	400 nm	3×10^{14} photons/pulse
Frequency tripling	267 nm	4×10^{13} photons/pulse
Nonlinear mixing	480–700 nm	1×10^{14} photons/pulse
Pulse length	150 fs	
Repetition frequency	896.6 Hz	

2. Optimization of a pump–probe experiment – the case of photolysis of molecular iodine

Unlike, for example, gas-phase reactions, solution chemistry includes the interaction of the reacting molecules with their solvation cage. This implies a strong interest in the study of diluted systems. A prominent model system consists of the photoexcitation of molecular iodine (Smith & Harris, 1987; Herzberg, 1991; Kelley *et al.*, 1984; Harris *et al.*, 1986). In solution, it is found that different time scales of dissociation, vibrational cooling, geminate recombination and cage breaking are delicately tuned by the solvent properties. At the same time, the process is described by the reaction coordinate that is parameterized by the I—I distance. This molecular bond length thus constitutes the 'order parameter' of the reaction and X-ray scattering. For instance, the geminate 'hot' molecular state (A/A′) is characterized by an increase of the 2.66 Å distance in the ground state to about 3.1 Å (Herzberg, 1991). This makes X-ray scattering a suitable tool for detecting such changes (Neutze *et al.*, 2001).

Nevertheless, the technique imposes several constraints on the experimental set-up. X-ray diffuse scattering contains the scattering from all the molecules hit by the beam without the possibility of discrimination between solute molecules and solvent background.

The signal in an ideal experiment will scale with the number of excited molecules, whereas the noise comes mainly from the Poisson statistics of the X-ray flux on the detector and therefore scales with the square root of the full scattering background (solvent and solute molecules). In order to maximize the (weak) signal above the (large) background, one could increase the concentration and the laser flux strongly or, at a given laser power, reduce the illuminated volume by focusing the laser further and reducing the X-ray aperture accordingly. Apart from fundamental considerations (*e.g.* the strong interaction of solute molecules at high concentrations) there are certain limits to be taken into account. We assume in the following that laser and X-ray beam impinge coaxially on the sample, which can be assumed to be a thin slab of (circulated) liquid perpendicular to the beam axis.

First the laser fluence should be limited to minimize two-photon absorption, *i.e.* the number of photons per area should not exceed the inverse of the absorption cross section of the solute molecules (3×10^{-21} m^2 for one iodine molecule). With the power of the present femtosecond source (see Table 1), the laser focus size should not be smaller than 0.1–0.2 mm^2. For probing this area, an X-ray spot size of 0.04 mm^2 is best suited to collect the largest possible scattering

† Presented at the 'ESF Exploratory Workshop on Time-Resolved Investigations with Neutrons and X-rays (TINX)' held in Berlin, Germany, in September 2001.

amplitude. Second, the concentration could still be increased by reducing the path length of the laser and X-rays with a constant number of photosensitive molecules illuminated. As we use either a capillary enclosed liquid jet or a free jet running in air, the scattering from the gas and/or capillary will exceed the scattering from a thin sheet of liquid when reducing the thickness. In the case of ethanol, 50 μm of film thickness is the limit for a free jet (500 μm for a jet in a capillary). These limits clearly define the typical excitation and probe volume for a given system. The number of photons available in a single laser pulse limits the number of molecules that can be excited. Therefore, the optimal concentration is set such that the absorbance of the sample is close to 1. In summary, such photoexcitation experiments have to be conducted in rather dilute solutions and with a probe volume of about 0.01 cm^3 for the present system. Here we present the study of 10 m*M* iodine in ethanol.

3. Diffuse scattering cross section

Scattering from disordered systems can be described in a straightforward fashion where the only relevant parameter is the momentum transfer of the scattered X-ray photons $Q = (4\pi/\lambda)\sin(2\theta/2)$, with wavelength λ and total scattering angle 2θ. Generally, the Fourier transform of the electron density distribution can be collapsed to the so-called Debye equation, where the intensity $I(Q)$ is expressed in electron units relative to the primary intensity (Warren, 1990),

$$I_{\rm eu}(Q) = \sum_m \sum_n f_m(Q) f_n(Q) \left[\sin(QR_{mn})/QR_{mn}\right], \qquad (1)$$

and where $f_{m,n}$ are the amplitudes formed by the atomic scattering functions and R_{mn} is the pairwise distance between two scatterers with positional correlation. The general shape of the distribution will have a maximum amplitude in the forward direction of $2Z^2$, where Z is the number of electrons in the molecule. Towards higher Q, it will fall off with $1/Q$ and the decay of the form factor of the atoms. The $\sin x/x$ function contains the structural information on the molecular arrangement as oscillations, the frequency of which is proportional to the inverse of the bond length. This formula is strictly valid only for scattering in gases. In an infinitely dilute solution, the solute molecules are considered to be completely disordered and not interacting with each other; therefore this formula is also applied to the difference scattering of solution and pure solvent. Elaborate theories implement the statistical mechanics and the quantum mechanics of the excitation process (Bratos *et al.*, 2002).

In dense disordered systems, a second level of positional correlation can be separated, besides the rigid positions of atoms within a molecule. A cross-correlation function $S(Q)$ describes the pair correlation in between different molecules (*e.g.* solute–solute or solute–solvent correlation). The intensity distribution is multiplied by this factor. Consequences of the intermolecular correlation are the low scattering intensity at low Q and prominent correlation peaks of nearest or next-nearest neighbors (see the scattering distribution of ethanol in Fig. 3). From the function $S(Q)$, the pair correlation function $g(r)$ in real space can be calculated. This describes the spatial arrangement of the molecules (Guinier, 1963). In general, these structural motifs can be clarified by a comparison with molecular dynamics simulations, in particular, those of the excited states (Bratos *et al.*, 2002; Vuilleumier & Mirloup, 2002).

If a detector without energy discrimination is used to collect the diffracted signal, additional contributions from inelastic processes can arise. The most prominent effect stems from the inelastic cross section with nearly free electrons, the so-called Compton scattering. This can be modeled by the excess between elastic scattering and the electron number of the atoms. It is found, to a good approximation, to be independent of structural properties,

$$I(Q) \propto Z - \sum_{n=1}^{Z} f_n^2(Q). \qquad (2)$$

Phenomenological expressions for the elements are given by Pálinkás (1973) and Hajdu (1972). Additionally, X-ray fluorescence following photoelectric absorption may occur if the excitation energy is above the characteristic edge of absorption of the elements under study. Fluorescence is unpolarized and isotropic, and the magnitude of the contribution can be measured. As both contributions are unmodified by structural rearrangements, they cancel out in difference maps of the excited state towards the non-excited state but are important in the absolute scaling of the scattering to derive quantitative fits to the experimental data.

We will now estimate numbers for the cross sections of the different constituents and the required signal-to-noise ratio for the photoexcitation studies. Consider a 0.01 mm^3 volume of ethanol, where 10 m*M* iodine are dissolved. This constitutes a typical solution that is used to match X-ray focus size and laser penetration depth. The concentration corresponds to one iodine molecule in 2.4×10^3 ethanol molecules. With the absolute scaling of the scattering cross section of N molecules and classical electron radius r_0,

$$\mathrm{d}I/\mathrm{d}Q = r_0^2 N I_0 I_{\rm eu}(Q) \frac{\pi}{2}(3 + \cos 2\theta), \qquad (3)$$

containing the space-angle conversion and polarization correction, we can expect, for an incoming intensity I_0 of 2×10^8 photons s^{-1}, about 4000 scattered photons s^{-1} from ethanol in a Q interval of 0.05 $Å^{-1}$ over a 2π integration in the azimuthal direction (fulfilled within a factor of two in a relatively large range of medium to high Q). This interval is chosen to allow the resolution of bond-length changes of iodine. The scattering from the iodine is lowered by the molecular fraction and Z^2(iodine)/Z^2(ethanol), *i.e.* the higher electron number scales up the scattering from high-Z solute molecules. This means that around 25 photons stem from the iodine molecules. The structural change after photoexcitation (*i.e.* in the A/A′ state) is again smaller than the full scattering from iodine. With the above formulae, we derive for the signal-to-noise ratio, defined as

$$\mathrm{S/N} = \Delta I_{\rm iodine}/(I_{\rm ethanol} + I_{\rm iodine}), \qquad (4)$$

a number ≤ 0.4 for a 1 s exposure when the ground state is changed to the expanded state A/A′. The assumption that 100% of molecules are excited is a hypothetical situation in femtosecond excitation; typically, one has to deal with 10–30% excitation. In order to derive reasonable S/N numbers with this degree of excitation, the exposure time has to be raised to 10^4 s. Taking into account drifts of set-up, sample and detector, such a measurement can take several hours to days, with still only one time point of the laser-to-X-ray delay being probed. For other photosensitive systems, the situation can be even more unfavorable. In previous studies with monochromatic X-ray scattering (Neutze *et al.*, 2001; Geis *et al.*, 2001), the signal-to-noise ratio was found to be only slightly above the calculated values.

4. Experimental set-up

The instrumentation at ID09B was originally designed for single-shot Laue experiments on macromolecular crystals (see, for example, Srajer *et al.*, 2001). The approach of using broadband X-ray sources together with submillimeter-sized samples and area detectors is found also to be ideal for diffuse scattering in solution. A detailed

description of the beamline can be found by Wulff *et al.* (1997), Schotte *et al.* (2002) and Techert *et al.* (2001).

The photoreaction can be initiated by a Ti:sapphire chirped pulse-amplifier system that runs at 896.6 Hz. This number is a subharmonic of the RF frequency in the storage ring of ESRF, which accelerates the electron bunches. The perfect mode lock is provided by a femtosecond Ti:sapphire oscillator with an actively tunable cavity (MIRA, coherent). Selected laser pulses are amplified by a diode-pumped Nd:YLF laser (Hurricane, Spectra Physics), which is *Q*-switched synchronously to the electron-pulse structure in the ring (see Fig. 1).

Time delays can be modified by electronically introducing delays in the trigger pulses. Two levels of delay for the laser pulse, with respect to the synchrotron time structure, are implemented to cover the time scale from picoseconds to milliseconds. First the phase of the femtosecond oscillator can be shifted with respect to the reference phase of the 88 MHz signal derived from the RF frequency. That induces pulse delays within a range of 11.6 ns and can be performed with 5 ps accuracy. For larger delays, a different femtosecond pulse is chosen out of the pulse train to be amplified in the amplification stage.

Alternatively, a *Q*-switched nanosecond laser (Quantel) can be used, which is synchronized by triggering the *Q* switch. The time delay between laser and X-ray pulses is probed by a GaAs photoconductor (Wrobel *et al.*, 1998) and can be calibrated with 10 ps accuracy. Experimental details are described elsewhere (Wulff *et al.*, 1997; Schotte *et al.*, 2002).

In order to obtain pairwise X-ray and laser pulses at the sample, the X-ray bunch train is chopped by a mechanical wheel possessing a long tunnel of small gap. The opening time of the chopper can be tuned according to the tunnel gap and rotation frequency, being between 300 ns and 1.4 µs for the 896.6 Hz operation. To take advantage of the natural 50–200 ps pulse length in the storage ring, fast structural studies are restricted to special filling patterns of the ring. In the so-called single-bunch mode, only one pocket (local energy minimum for electrons in the RF potential) out of 992 possible ones is filled with a high number of electrons. Thus, the time spacing of subsequent X-ray pulses is 2.8 µs, equal to the revolution time of the electron bunches in the ring. In the 16-bunch mode, 16 individual pockets of equal spacing are filled up, reducing the distance between two subsequent pulses to 176 ns. Hybrid modes are possible with partial homogeneous filling opposite single bunches. The spacing in the 16-bunch mode still allows an extraction of single pulses, using a small aperture in the chopper tunnel of 145 µm, but only at the expense of flux.

This system allows us to run stroboscopic excitation experiments with detectors without time resolution (two-dimensional detectors). The duty cycle of the chopper thus drastically reduces the usable flux by a natural factor of 396 in the single-bunch mode up to 6336 plus spatial transmission losses for the 16-bunch mode with respect to the incident flux.

Furthermore, millisecond shutters for the laser and X-rays enable real one-shot acquisition or reduced stroboscopic frequencies. The X-ray shutter is also used to define the exposure time on the two-dimensional detector.

In a typical liquid-scattering experiment, a liquid jet is prepared either in a glass capillary or as a free laminar jet from a nozzle. The scattering is recorded on a CCD camera (MarCCD) allowing a good spatial resolution. Alternatively, an annular gas detector without spatial resolution can be used. This allows a time resolution of 100 ns, which is suitable for lock-in techniques.

5. Characteristics of the X-ray source

The X-ray optics consist of an optional Si(111) channel-cut monochromator that is cooled by liquid nitrogen and accepts a high heat load from the source. Afterwards, the beam is focused by a toroidal mirror using a moderate demagnification ($M = 0.68$) to produce a 0.45 mm focal spot at the sample. An upgrade with a superior slope error is expected to give a spot size below 150 µm.

The X-ray source consists of several multipole devices from a broadband wiggler to the single-line undulator that is of interest within this article. It consists of 162 poles of NdFeB permanent magnets with a period of 20 mm (therefore called U20). The important values for insertion devices are the critical energy $E_{\rm crit}$ and the energy of the harmonics to the period E_n (both in keV) in relation to the electron energy E (in GeV),

$$E_{\rm crit} = 0.245 E^2 B_0 \tag{5}$$

and

$$E_n = 0.95 \frac{nE^2}{\lambda_0[1 + K^2/2 + (\gamma\Theta)^2 + (\gamma\Phi)^2]}, \tag{6}$$

which already includes the effects of out-of-orbit angles Θ and Φ present at some aperture slits. Further parameters are the magnetic period λ_0 (units cm), the deflection parameter $K = eB_0\lambda_0/(2\pi mc)$ for a magnetic field maximum at the electron trajectory B_0 (units T), and electron charge and mass e and m, respectively. The deflection parameter K determines the way that X-ray photons emitted along different points along the electron trajectory interact, and it can be imagined as the angular limit for tangents on the sinusoidal electron trajectory. For values of K larger than the relativistic emission cone opening $1/\gamma$, the X-ray intensity adds up incoherently and a broad energy emission results. Conversely, if the deflection parameter is smaller, photons will interfere constructively forming distinct peaks in the spectrum. Additionally,

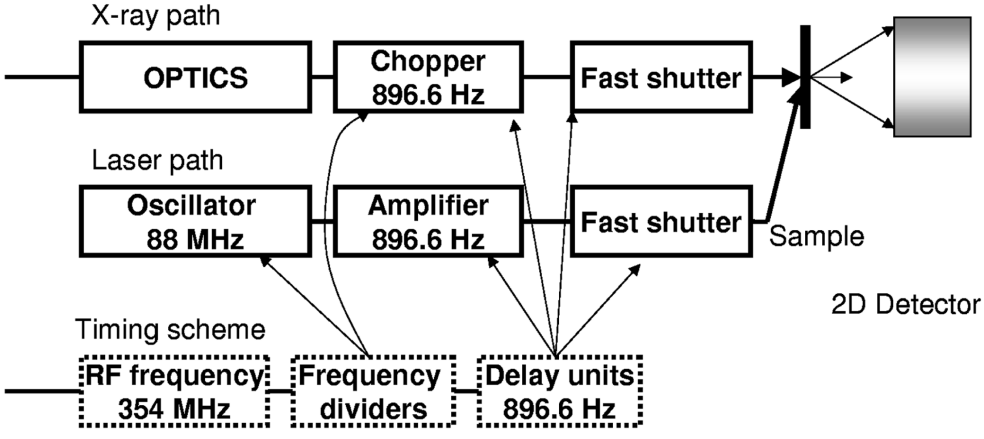

Figure 1
Schematic diagram of the control of beamline elements and the laser system by the RF frequency of the storage ring.

Table 2
Characteristic parameters for single-line undulators in use at ESRF suitable for white-beam diffuse scattering studies.

The power P and the harmonic energies are given for the smallest accessible gap.

	U20	U17
Magnetic period λ_0 (mm)	20	17
K	0.27	0.86
Poles	163	235
Minimum gap (mm)	16.3	6
B_0 (T)	0.146	0.544
E_{crit} (keV)	3.5	13.2
E_1 (keV)	16.7	14.8
E_2 (keV)	39.3	29.0
E_3 (keV)	52.8	44.5
P (W/A)	80/0.1	1370/0.1

the relative magnitudes of critical energy and harmonic energy under consideration determine the purity of the undulator line. In order to obtain a pure narrow spectrum around the harmonic energy the critical energy should be much lower. For a trade-off between purity and flux, meanwhile, a compromise has to be used. Table 2 gives the parameters for the U20 device at ID09B and those of a scheduled upgrade to an in-vacuum undulator with a 17 mm period.

Clearly, the maximum magnetic field influences the harmonic energies, but it also increases the emission efficiency of the device. By lowering the gap between the opposite magnet arrays the field is tuned so that energy tunability of the lines is enabled. Furthermore, the real spectrum of the devices depends on the acceptance angles by the first slits in the beamlines, which are 27 m away from the source point in our case. We will not give the full formulae, but rather refer to numerical programs that are available, such as *XOP* (Dejus & Sánchez del Río, 1996), which was used to calculate the spectra shown in Fig. 2.

The first harmonic is very strong in the case of a small critical energy, whereas the second harmonic is forbidden on the symmetry axis but occurs as a broad distribution with a finite aperture and vertical electron-trajectory divergence. The third harmonic is again sharp and can be rejected by our platinum-coated mirror. In summary, the present insertion device can give a predominant single line on the first harmonic, the spectral purity of which will be discussed below.

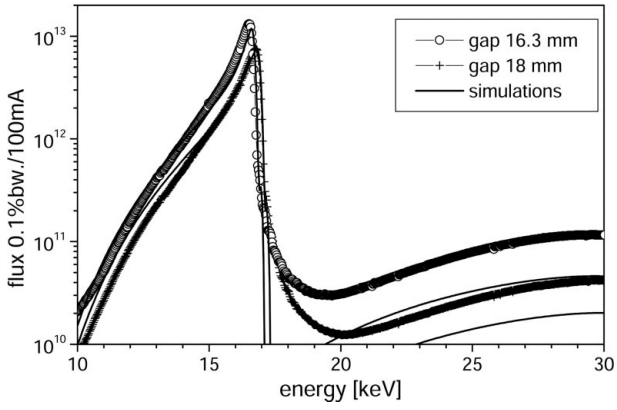

Figure 2
Spectral distribution of radiation emission from the U20 undulator for two different gap settings. The lines correspond to numerical calculations using the software package *XOP*. Some deviations at high energy stem from bending-magnet background radiation.

6. Demonstration of the scattering from a solution

So far, the flux from the U20 device and an Si(111) channel-cut with 2×10^8 photons s^{-1} have been considered. The choice of the steps in Q resolution (0.05–0.10 Å^{-1}) already indicates the level of resolution that is needed. Generally speaking, the resolution in momentum transfer has to be the same as that desired for the resolution in bond-length change. Therefore, the flux of the full undulator line can be used in our case without considerable loss of information. To demonstrate the effect, we will compare the scattering distribution from an iodine/ethanol solution in both the monochromatic and the polychromatic set-up. We used a non-chopped beam of size 200×200 µm and exposed a 300 µm-thick free jet for 30 s. For the polychromatic exposure, the slit size was reduced to account for the increased flux level. The scattering was collected on a MarCCD camera (consisting of a scintillator screen, fiber optics and a 16-bit cooled CCD chip having 2048×2048 pixels). The two-dimensional intensity was integrated azimuthally to derive the radial distribution function as a function of Q. The software (Hammersley *et al.*, 1996) allows correction for space-angle and polarization distortion.

Fig. 3 displays both experimental curves together with a fit to the polychromatic measurement. For that purpose, the monochromatic scattering curve is convoluted with the spectral-line distribution of the radiation source. We find a perfect match within a large Q range. Only the region of momentum transfer below the liquid peak is altered considerably (see inset of Fig. 3) and cannot be fitted by the first-harmonic line of the undulator alone. We also had to take into account the weak distribution of the suppressed second harmonic, which gives excess scattering from the liquid peak at half the solid angle. Thus, a good simulation of the polychromatic scattering distribution is achieved showing the predictability of the profile. The higher-order contamination is less critical for the signals of the photoexcitation, as it cancels out for difference measurements and the difference signal due to the second-harmonic flux is much lower than the first-harmonic signal.

The important result is a gain in flux of 100–500 depending on the slit settings. The spectral purity of the undulator line can be tuned by the vertical aperture of the defining slits by reducing off-axis

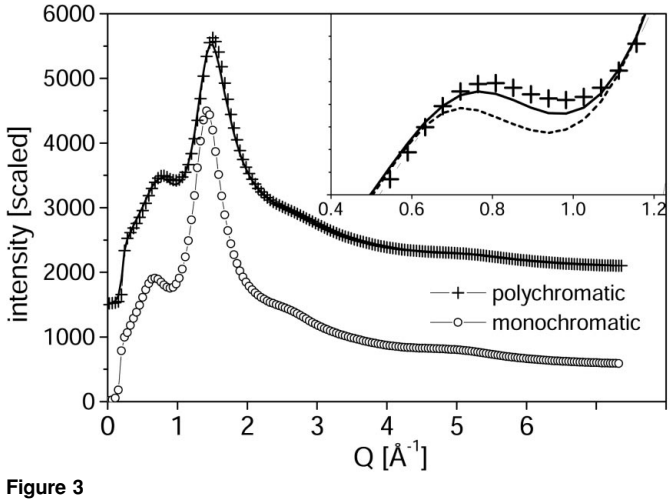

Figure 3
Scattering distribution function for an ethanol–iodine solution in both monochromatic (circles) and polychromatic (crosses) set-ups. The polychromatic curve is shifted up by 1500 in intensity units for clarity. The lines are a convolution of the monochromatic scattering profile with the line shape of the undulator radiation source. The dashed line uses only the first harmonic, whereas the full line takes into account the harmonic contamination. The inset magnifies the deviation at low Q.

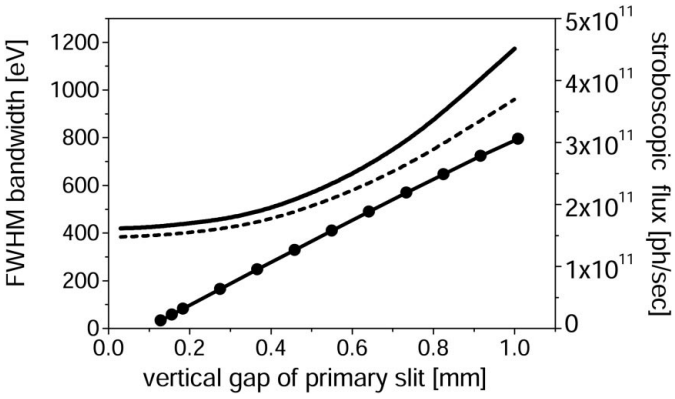

Figure 4
Calculated bandwidth for the first harmonic of the U20 undulator as a function of the vertical acceptance by the first downstream slits in terms of the opening gap. The dashed line corresponds to the additional effect of an aluminium filter. The line with circles displays the stroboscopical flux on the sample.

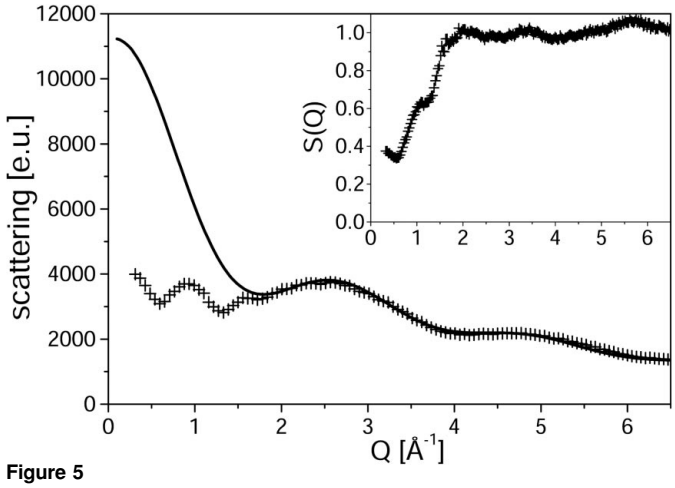

Figure 5
Scattering distribution function of gas-like iodine molecules in ethanol solution obtained *via* subtraction of the ethanol scattering. The line is a calculation of the molecular structure function according to (1). The inset shows the extraction of the intermolecular correlation function.

contributions. The full width at half-maximum (FWHM) has been calculated as a function of the slit settings in Fig. 4. The influence of an aluminium filter is also introduced. The flux is reduced linearly in the central cone of the radiation.

Opening the undulator gap does not influence the bandwidth but shifts the energy of the first harmonic and damps the magnitude of the second harmonic. Thus the desired bandwidth *versus* flux can be optimized to meet the requirements of the system under study.

To demonstrate the reliability of the technique, we show the difference spectrum of the iodine solution to the spectrum of pure ethanol in the polychromatic mode as already discussed above. The result should represent the pure-gas scattering function of the iodine molecules. Indeed, the oscillations at high Q perfectly fit the distribution as calculated from (1). We used a ground-state distance of the iodine atoms of 2.66 Å and convoluted the monochromatic function with the spectrum of the undulator.

In contrast, at low Q we observe significant deviations of the experimental curve from the simulation. These can be attributed to intermolecular cross correlation [$S(Q)$ resembling hard-core systems, see inset of Fig. 5]. An important underlying effect can be related to the formation of a solvation shell around an iodine molecule as has been manifested in recent molecular dynamics studies (Vuilleumier & Mirloup, 2002). The peak at around 0.9 Å can be explained by a first solvation shell of radius 4 Å. Although this is a static structure function derived in equilibrium for a non-perturbed sample, we can expect to resolve structural details about the molecular excitation of small molecules as well as the reaction of the solvation structure with unprecedented precision and for the first time obtain complete time-delay series of photoinduced changes on a picosecond time scale.

7. Conclusion and outlook

Seminal studies have shown that X-ray probe photoexcitation studies in liquid solution are feasible. So far, limitations from the relatively low usable flux in monochromatic scattering studies have limited the number of unique results in these studies. Relaxing the bandwidth of the X-ray source is shown to deliver the necessary flux to enable systematic studies. A gain of around 500 can reduce considerably the exposure time or allow studies of weakly scattering systems.

Scheduled refurbishments at ID09B are expected to further improve the flux gain by operating a single-line undulator in a vacuum with reduced magnet gap together with improved focusing optics. Currently, the heat load on the X-ray chopper limits the ultimate usable flux. The more important harmonic contamination of the new insertion device will necessitate further band-pass optics such as a reflective mirror or even multilayer mirrors.

Studies that use an X-ray streak camera would even become possible at the projected flux. This detector can further reduce the time resolution to below 1 ps (Naylor *et al.*, 2001) with a severe penalty in detection efficiency. With this resolution, a new region can be accessed that would allow the resolution of coherent nuclear motion. Similarly, the bandwidth of the undulator is well suited for other techniques where flux requirements are more important than resolution, as in small-angle scattering (Pollack *et al.*, 2001). Since in small-angle scattering the contribution of the solute molecules can be comparable with that of the solvent, the signal could be deduced even for weakly scattering systems. Estimates based on Guinier (1963) suggest it will be possible to observe a 5% change in the radius of gyration of, for example, hemoglobin molecules (radius of gyration 23 Å, density 1.33 g cm^{-3}) of 10 mM concentration in water within exposure times of minutes.

Future femtosecond X-ray sources such as energy-recovery Linacs or free-electron lasers may also provide intense pulses from undulator insertion devices to allow the study of photochemistry below the picosecond timescale.

References

Bratos, S., Mirloup, F., Vuilleumier, R. & Wulff, M. (2002). *J. Chem. Phys.* In the press.

Dejus, R. J. & Sánchez del Río, M. (1996). *Rev. Sci. Instrum.* **67**, 1–4.

Geis, A., Bouriau, M., Plech, A., Schotte, F., Techert, S., Trommsdorff, H. P., Wulff, M. & Block, D. (2001). *J. Lumin.* **94/95**, 493–498.

Guinier, A. (1963). *X-ray Diffraction in Crystals, Imperfect Crystals and Amorphous Bodies.* New York: Dover.

Hajdu, F. (1972). *Acta Cryst.* A**28**, 250–252.

Hammersley, A. P., Svensson, S. O., Hanfland, M., Fitch, A. N. & Hausermann, D. (1996). *High Press. Res.* **14**, 235–248.

Harris, A. L., Berg, M. & Harris, C. B. (1986). *J. Chem. Phys.* **84**, 788–806.

Herzberg, G. (1991). *Molecular Spectra and Molecular Structure*, Vol. I, *Spectra of Diatomic Molecules.* Malabar: Krieger.

Kelley, D. F., Abul-Haj, N. A. & Jang, D. (1984). *J. Chem. Phys.* **80**, 4105.

Naylor, G. A., Scheidt, K., Larsson, J., Wulff, M. & Filhol, J. M. (2001). *Meas. Sci. Technol.* **12**, 1858–1864.
Neutze, R., Wouts, R., Techert, S., Davidsson, J., Kocsis, M., Kirrander, A., Schotte, F. & Wulff, M. (2001). *Phys. Rev. Lett.* **87**, 195508-1–195508-4.
Pálinkás, G. (1973). *Acta Cryst.* A**29**, 10–12.
Pollack, L., Tate, M. W., Finnefrock, C., Kalidas, C., Trotter, S., Darnton, N. C., Lurio, L., Austin, R. H., Batt, C. A., Gruner, S. M. & Mochrie, S. G. J. (2001). *Phys. Rev. Lett.* **86**, 4962–4965.
Schotte, F., Techert, S., Anfinrud, P. A., Srajer, V., Moffat, K. & Wulff, M. (2002). *Third-Generation Hard X-ray Synchrotron Radiation Sources*, edited by D. Mills. New York: John Wiley.
Smith, D. E. & Harris, C. B. (1987). *J. Chem. Phys.* **87**, 2709–2715.
Srajer, V., Ren, Z., Teng, T. Y., Schmidt, M., Ursby, T., Bourgeois, D., Pradervand, C., Schildkamp, W., Wulff, M. & Moffat, K. (2001). *Biochemistry*, **40**, 13802–13815.
Techert, S., Schotte, F., Plech, A., Eybert, L., Geis, A. & Wulff, M. (2001). *Proceedings of the Winterschool Les Houches 2001*. Berlin: Springer.
Vuilleumier, R. & Mirloup, F. (2002). In preparation.
Warren, B. E. (1990). *X-ray Diffraction.* New York: Dover.
Wrobel, R., Brullot, B., Dainciart, F., Doublier, J., Eloy, J.-F., Marmoret, R., Villette, B., Mathon, O., Tucoulou, R. & Freund, A. K. (1998). *Proc. SPIE*, **3451**, 156–163.
Wulff, M., Schotte, F., Naylor, G., Bourgeois, D., Moffat, K. & Mourou, G. (1997). *Nucl. Instrum. Methods Phys. Res. A*, **398**, 69–84.

 Received 19 December 2001 • Accepted 24 June 2002